Broadband graphene based electro-optic chiral polarization conversion for terahertz pulse shaping

Zefeng Chen[1, 2, 3]#, Xuequan Chen[4]#, Li Tao[5]#, Kun Chen[6], Rui Zhang [7], Mingzhu Long[8], Emma Pickwell-MacPherson[9,]*, and Jianbin Xu[3,]*

1. School of Optoelectronic Science and Engineering and Collaborative Innovation Center of Suzhou Nano Science and Technology, Soochow University, Suzhou 215006, China
2. Key Lab of Advanced Optical Manufacturing Technologies of Jiangsu Province & Key Lab of Modern Optical Technologies of Education Ministry of China, Soochow University, Suzhou 215006, China
3. Department of Electronic Engineering, The Chinese University of Hong Kong, Hong Kong, Shatin, NT, Hong Kong SAR, China
4. Great Bay Area Branch of Aerospace Information Research Institute, Chinese Academy of Sciences, Guangzhou 510530, China
5. Key Lab of Advanced Optoelectronic Quantum Architecture and Measurement (MOE), School of Physics, Beijing Institute of Technology, Beijing 100081, China
6. State Key Laboratory of Optoelectronic Materials and Technologies, School of Electronics and Information Technology and Guangdong Province Key Laboratory of Display Material, Sun Yat-sen University, Guangzhou 510275, China
7. Shenzhen Institute of Advanced Technology, Chinese Academy of Science, Shenzhen 518000, China
8. South China Academy of Advanced Optoelectronics, South China Normal University, Guangzhou, 510006, China.
9. Physics Department, Warwick University, Coventry CV4 7AL, UK

# These authors contributed equally to this work.

*To whom all correspondence should be addressed. Email: jbxu@ee.cuhk.edu.hk and e.pickwell.97@cantab.net

Abstract:

Terahertz(THz) radiation is ideally suited for non-invasive testing and short-distance data transmission. Active controlling the polarization of THz wave is highly desirable in measurement systems. Although significant developments of THz active devices had been achieved through introducing electromagnetic resonance structure (e.g. metamaterials), the bandwidth is limited. Here we propose a graphene-based electrically reconfigurable polarization conversion across a broadband THz region (0.3 THz to 0.9 THz) for controlling the chiral polarization of terahertz pulse. By electrically controlling the graphene conductivity, we can switch the device reflection in-between total internal reflection and metal mirror reflection to realize a frequency-independent phase change, which enables a tunable waveplate with high dynamic range for manipulating the polarization of THz wave. Due the frequency-independent modulation property, we achieved tunable chiral polarization THz waveforms in the time domain for the first time, from right-handed to left-handed polarization. This work opens up a new mechanism for designing novel THz modulators for THz circular dichroism.

Keywords: terahertz, broadband modulation, chiral polarization, graphene, pulse shaping

1.1 Introduction

THz or submillimeter waves have attracted attention due to their potential applications in time-domain far-infrared spectroscopy, investigations of ultrafast dynamics in materials[1,2] and wireless communication [3-5]. Specifically, active modulation of the chiral polarization states of terahertz light is a requirement for a wide range of photonic processes such as non-contact Hall measurements[6], circular dichroism sensing of chiral molecules and proteins[7-9] and anisotropy imaging[10]. To actively control the polarization, two key properties are required simultaneously for a device: a material with tunable complex refractive and in-plane symmetry breaking to generate phase difference between two orthogonal EM wave. The former can be achieved through liquid crystal [11], or tunable free carrier absorption of semiconductor[12,13]. The latter one can be achieved through nanostructured metasurface elements [14-16].

Despite important advances in the exploration of the active control of polarization, electrical control of THZ chiral polarization remains largely elusive and suffers from limited dynamic range of polarization conversion and limited response frequency bandwidth [17-20]. Due to the highly tunable conductivity in THz region, 2D materials (e.g. graphene and black phosphorus) show great potential in THz modulation[21-25]. Combining graphene with metamaterials/metasurface, electrical modulation of polarization state of THz beams has been widely demonstrated [25-46]. However, the working frequency is limited at a certain narrowband due to the resonance nature of metamaterial.

Here we report a graphene-based electrically reconfigurable polarization conversion across a broadband THz region (0.3 THz to 0.9 THz) for controlling the chiral polarization of terahertz pulse. Utilizing the highly tunable conductivity of graphene, the device can be switched between total internal reflection (TIR) and metal mirror reflection (MMR), which provides a highly tunable phase difference of 140° between two orthogonal EM wave components, providing a tunable waveplate with high dynamic range. With this device the polarization of THz wave can be conversed from right-handed circular polarization, to linear polarization, then to left-handed circular polarization under different gate voltages, demonstrating versatility with a high dynamic range. More

importantly, because of the frequency–independent property of TIR and MMR, this device has ultra-broadband response property.

Physical model

A graphene sheet is placed at the interface of two media with refractive indexes of n_1 and n_2 with $n_1>n_2$, and THz light is incident from n_1 to n_2, as shown in figure 1a. We use an example of a reflection from the quartz-air interface with $n_1=2$ and $n_2=1$. The reflection coefficients for *s*-polarization light can be expressed as:

$$r_s = \frac{n_1 \cos\theta_i - i \cdot \sqrt{n_1^2 \sin^2\theta_i - n_2^2} - Z_0\sigma_s}{n_1 \cos\theta_i + i \cdot \sqrt{n_1^2 \sin^2\theta_i - n_2^2} + Z_0\sigma_s} \quad \text{Eq. (1)}$$

where n_1 is the refractive index of the incident medium, θ_i is the incident angle, n_2 is the refractive index of the refraction side medium, Z_0 is the vacuum impedance (377 Ω) and σ_s is the sheet conductivity of graphene. According to previous reports, the conductivity of monolayer graphene can be tuned to several micro siemens[47-49]. In this idea physical model, we assume that the conductivity is from 0mS to 10mS. The detailed derivation process is shown in the supporting information (S1). When the incident angle θ_i equals the TIR angle θ_c ($\theta_c = arcsin\frac{n_2}{n_1}$), the reflection coefficient becomes a pure real number and can be switched from positive to negative by increasing the conductivity of graphene, which means that the reflection phase shift will jump from 0 to 180° (or -180°). As shown in figure 1(b), the reflection phase is zero and the amplitude decreases as the conductivity increases, when $Z_0\sigma_s < n_1 \cos\theta_c$; and the phase jumps to 180° and the amplitude increases as the conductivity keeps increasing to make $Z_0\sigma_s > n_1 \cos\theta_c$. This phenomenon is easy to be understood from the physical picture as shown in figure 1(c). The reflection of this system can be considered as the competition between TIR and MMR depending on the conductivity of the interface. If the conductivity of graphene is high enough(σ_g>>4.6mS), the reflection is dominated by the MMR, with reflection phase of 180° (bottom of figure 1(c)). Otherwise, the reflection system returns to TIR with a phase shift of zero, (top of figure 1(c)). Specifically, when their reflection amplitudes are equal, the reflection coefficient of the system is zero, and the incident THz wave is lost as Joule heating. In the process of TIR to MMR, the reflection coefficient changes from the first to second quadrant in the complex plane, as shown in the inset of figure 1(b). This enables large phase modulations up to 180°. However, the phase change is not continuous and has an abrupt jump at the conductivity where the reflection reaches zero. This problem can be solved by setting $\theta_i > \theta_c$. For example, the reflection phase and amplitude as a function of conductivity when $\theta_i = 45°$ are calculated and shown as the red lines in figures 1(d) and (e). The phase of the s-polarization curve still decreases with conductivity but it varies continuously from -72° to -175°, leaving a phase modulation potential of 100°. Moreover, the reflection amplitude does not attenuate to zero with a minimum reflection of 0.32. We call this phase change with non-zero amplitude a "pseudo phase transition".

$$r_p = \frac{i \cdot n_1\sqrt{n_1^2 \sin^2\theta_i - n_2^2} - n_2^2 \cos\theta_i - i \cdot Z_0\sigma_s \cos\theta_i \sqrt{n_1^2 \sin^2\theta_i - n_2^2}}{i \cdot n_1\sqrt{n_1^2 \sin^2\theta_i - n_2^2} + n_2^2 \cos\theta_i + i \cdot Z_0\sigma_s \cos\theta_i \sqrt{n_1^2 \sin^2\theta_i - n_2^2}} \quad \text{Eq. (2)}$$

For the p -polarization light, the reflection coefficients can be expressed as equation (2). When

$\theta_i = \theta_c$, the reflection coefficient is a pure real number, and is independent of the conductivity of graphene. However, when $\theta_i > \theta_c$, a similar phase change with conductivity can be observed. The reflection amplitude and phase at $\theta_i = 45°$ are shown as the blue curves in figure 1(d) and (e), respectively. The minimum reflection amplitude is 0.18 at the conductivity of 8mS. The phase can be tuned with a range of 110° from 42° to 150° with the conductivity increases from 0 to 10 mS.

As s- and p-polarizations are orthogonal, the projection of electrical vector trajectory of the composed THz EM wave can be descripted as $\frac{E_x^2}{E_p^2} + \frac{E_y^2}{E_s^2} - \frac{2E_xE_y}{E_pE_s}\cos\Delta\varphi = \sin^2\Delta\varphi$, where $\Delta\varphi$ is the phase difference of s- and p-polarization light. Obviously, the polarization of the composed THz wave become controllable as the phase different and amplitude ratio of the s-/p- polarization, which can be controlled by the conductivity of graphene. As shown in figure 1(f), as the conductivity of graphene increase from 0 mS to 10 mS, the phase difference can be tuned from 110°to 350°, while the amplitude ratio is from 1 to 1.25, then to 0.45. Because the phase difference over crosses 180°, the THz wave can be switched to different handedness elliptical polarization. Specially, when the conductivity of graphene is around 4.3mS, the phase different is 180°, then THz wave becomes linearly polarized.

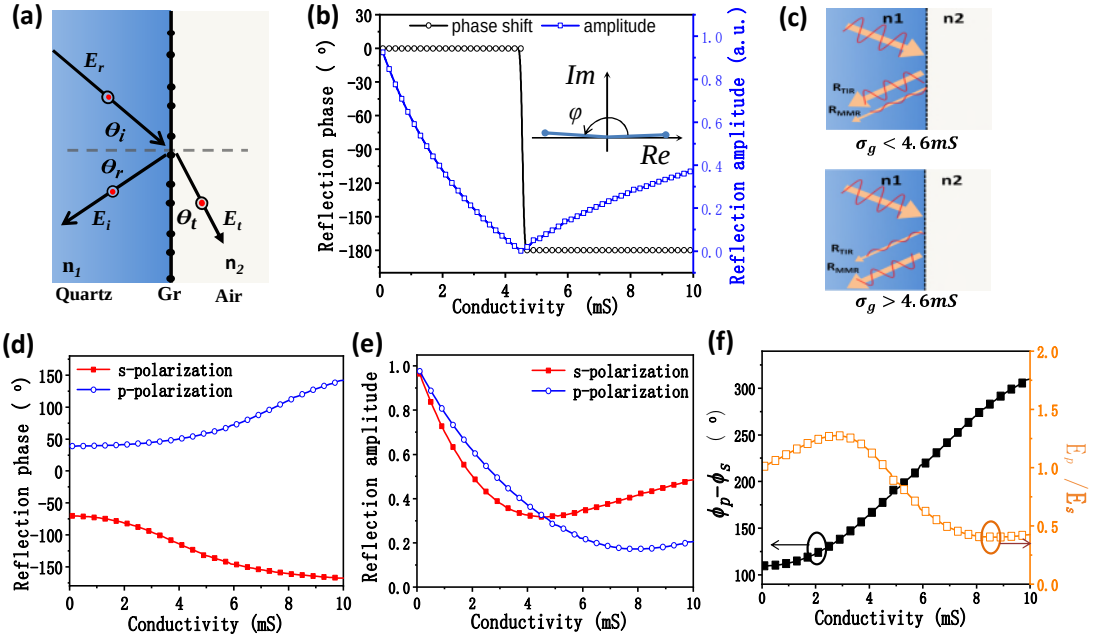

Figure 1 (a) Optical path diagram of the incident light from quartz to air (b) The theoretical reflection phase and amplitude as a function of conductivity, when the light is incident at the critical angle, the inset shown the reflection coefficient switching from positive to negative. (c) Schematic diagram of phase change effect on reflection system. TIR dominated (up) if the interface conductivity is low. MMR dominated (down) if interface conductivity is high enough. (d) Reflection phase shift and (e) amplitude variation for *p*- and *s*- polarization when $\theta_i = 45°$. (f) Phase difference and amplitude ratio between *p*- and *s*- reflections as a function of the graphene conductivity, when $\theta_i = 45°$.

1.3 Experiment

To prove the above concept, we used a 45° fused quartz prism to introduce a TIR incident angle.

Figure 2(a) is a schematic diagram of the device. Figure 2 (b) shows the cross-section of the reflection system. The THz light is normally incident into the prism, resulting in an incident angle of θ_i=45° to the quartz/graphene interface, which is larger than the TIR angle of arcsin n_2/n_1 =30°. Figure 2(c) is a photograph of the graphene/quartz component. To achieve higher conductivity of graphene, two 1 cm × 1 cm monolayer graphene sheets are transferred one by one and stacked on the top of quartz substrate. To tune the conductivity of the graphene, we used ion-gel as a side gate. Conventional graphene transistors, which tune the conductivity by the bottom or top gate, is not suitable for our device because the reflection from the top or bottom gate electrode will interfere the reflection from the graphene. To address this issue, we used a side gate geometry with an ion-gel film on top of the graphene to tune the conductivity of graphene. Ion-gel film is composed of organic framework (poly (vinylidene fluoride) / ethylene- vinyl acetate copolymer (PVDF/EVA)) and ionic liquid (1-ethyl-3-methylimidazolium bis(trifluoromethylsulfonyl)imide ([EMIM][TFSI])), with a subwavelength thickness around 100 μm, making it transparent to the THz waves. Therefore, this ion-gel side gate has a negligible effect on the TIR reflection. (Details about the fabrication process can be found in the method and supporting information). The Ion-gel film is placed on graphene as side gate (detail of fabrication process shown in the method and supporting information). The thickness and Raman spectrum of graphene after cover ion gel is shown in supporting information S2.

Before the THz measurement, we examined the electrical properties of the graphene through characterizing the transfer curve of the graphene as a field-effect transistor (the detail of graphene field-effect transistor is shown supporting information S4). The transfer curve of graphene with the ion gel as the side gate is shown in figure 2(d). Like previous reports, graphene shows a general p-type doping property, and the carrier neutral point is found at 0.4 V with a minimum conductivity of about 0.9 mS. At the gate voltage of about -1.5 V, the conductivity is tuned to about 7mS. The broad tuning range of the conductivity meets the requirement of the above physical model.

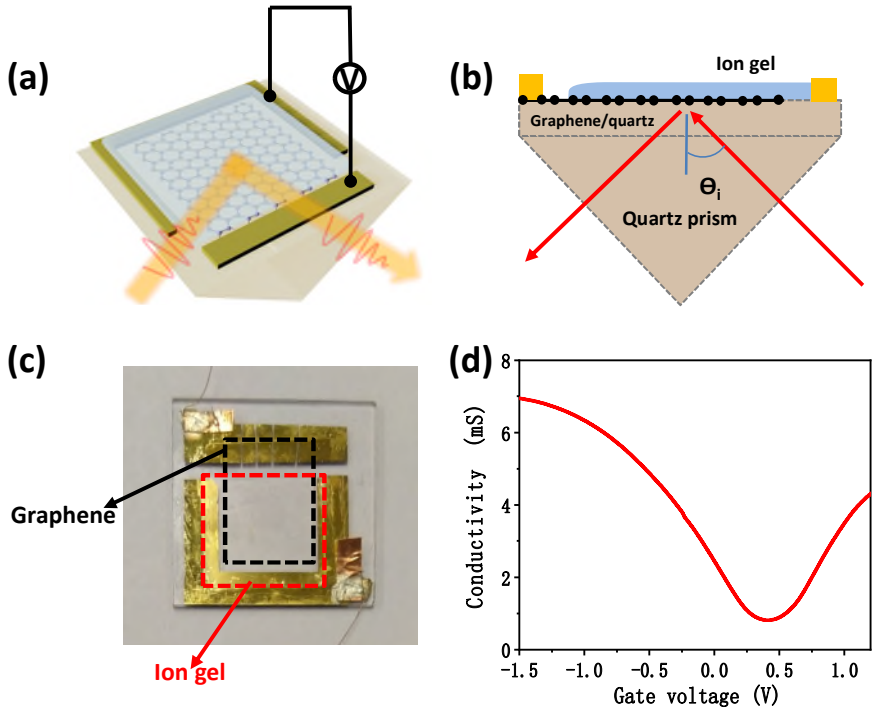

Figure 2 (a) schematic diagram of the graphene polarization converter (b) cross-section of the

reflection measurement geometry. (c) Photograph of the device (d) Transfer curve of the graphene-FET with ion-gel gate.

Results and discussion

Figure 3(a) shows the s-polarization reflection of the time-domain THz pulses with the gate voltage ranging from 0.4 V to -1.4 V. As the gate voltage decreases, the peak to peak value of the waveform decreases and then increases after -0.4 V. The pulse shape changes with the voltages as well. The reflectivity and the phase spectra with varied gate voltages are extracted from the reflected time-domain pulses by Fourier transform, as shown in Figure. 3(b) and 3(c), respectively. Using the spectrum at Vg = 0.4 V as the reference, the phase shift is around 80^{o} over a bandwidth of 0.6 THz (that is, 0.3–0.9 THz). In an ideal physical model, the phase shift is frequency independent. The actual phase slightly increases with frequency which is thought to be caused by the small dispersion of the graphene conductivity. The relative reflectivity is also broadband tunable, as shown in figure 3(c). According to figure 2(d), the conductivity of graphene is corresponding to the gate voltage. Through converting the gate voltage to conductivity, the phase shift and reflectivity can be plotted as function of conductivity, as shown in figure 3(d). Here, the result of 0.6 THz is taken as an example. The phase shift decreases with the conductivity monotonously; while the reflectivity decreases quickly first with the conductivity and then increases slowly after 5 mS. Obviously, the conductivity of around 5 mS (gate voltage of -0.6 V) corresponds to the pseudo phase transition point for this system. When the conductivity is smaller than 5 mS (gate voltage of 0.4V to -0.6V) the reflection system is dominated by TIR. When the conductivity is larger than 5 mS (gate voltage of -0.6 V to -1.4 V) the reflection system is dominated by MMR. These results agree well with the theoretical model mentioned above.

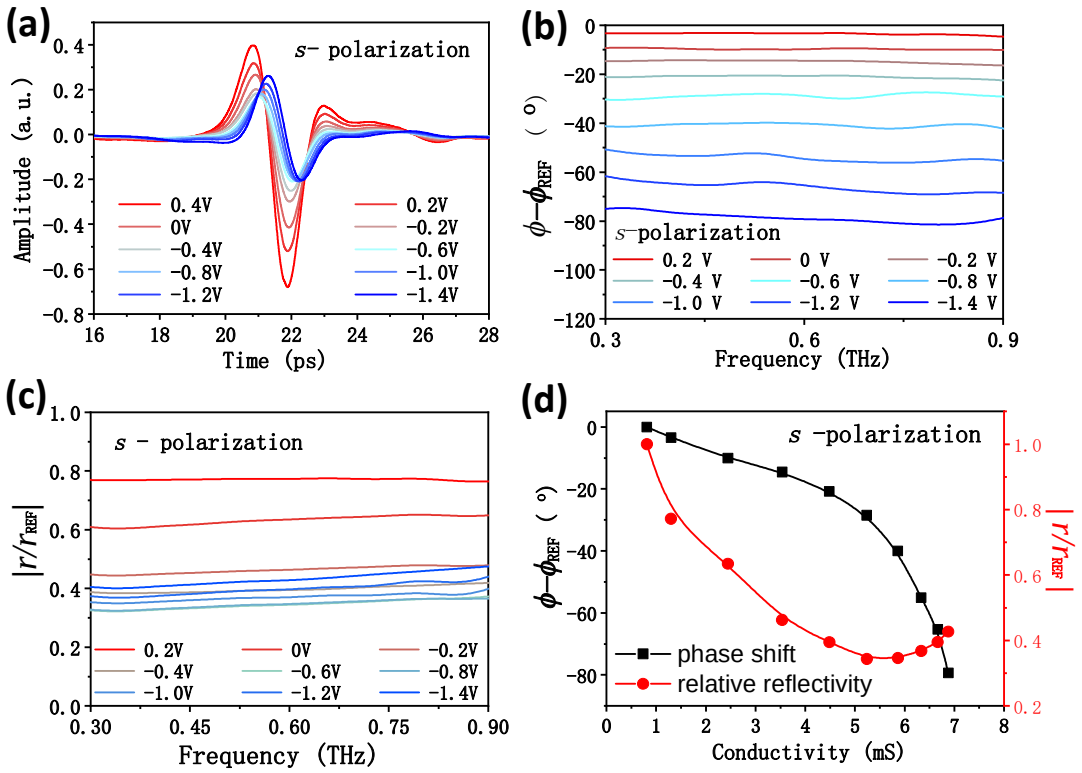

Figure 3 (a) Time domain THz waveforms of s-polarization under different gate voltages. (b) Phase modulations and (c) reflection intensity ($|r|$) modulation. Data are obtained by taking the Fourier

transforms of the signals in (a) and using the result at the gate voltage of 0.4 V as a reference. (d) reflection intensity and relative reflectance as a function of conductivity.

Figure 4(a) shows the p-polarization reflection of time-domain THz pulses. As the gate voltage decreases, the peak-to-peak amplitude of waveform decreases. The reflectivity and phase spectra at different gate voltages are shown in Figure 4(b) and 4(c), respectively. Again, the spectrum at the Dirac point (Vg = 0.4 V) is used as the reference. The phase shift is around 50° over a bandwidth of 0.6 THz (from 0.3 THz to 0.9 THz). Under a gate voltage of -1.4 V, the phase shift is 45° at the frequency of 0.3 THz, while it changes to 60° at 0.9 THz. The is because as the conductivity approaches 7 mS at -1.4 V, the phase shift is more sensitive to the dispersive conductivity of the graphene, which can be seen from Figure 1(d). The relative reflectivity decreases over this broadband region, as shown in figure 4(c). Figure 4(d) is the reflectivity and phase shift at 0.6 THz as a function of conductivity. As the conductivity increases, the phase shift increases and reflectivity decreases, which agrees well with the theoretical model. This monotonous decrease of reflectivity also indicates the reflection system is dominated by TIR. This is because in p-polarization, the conductivity of graphene is not high enough to make MMR sufficiently stronger than TIR.

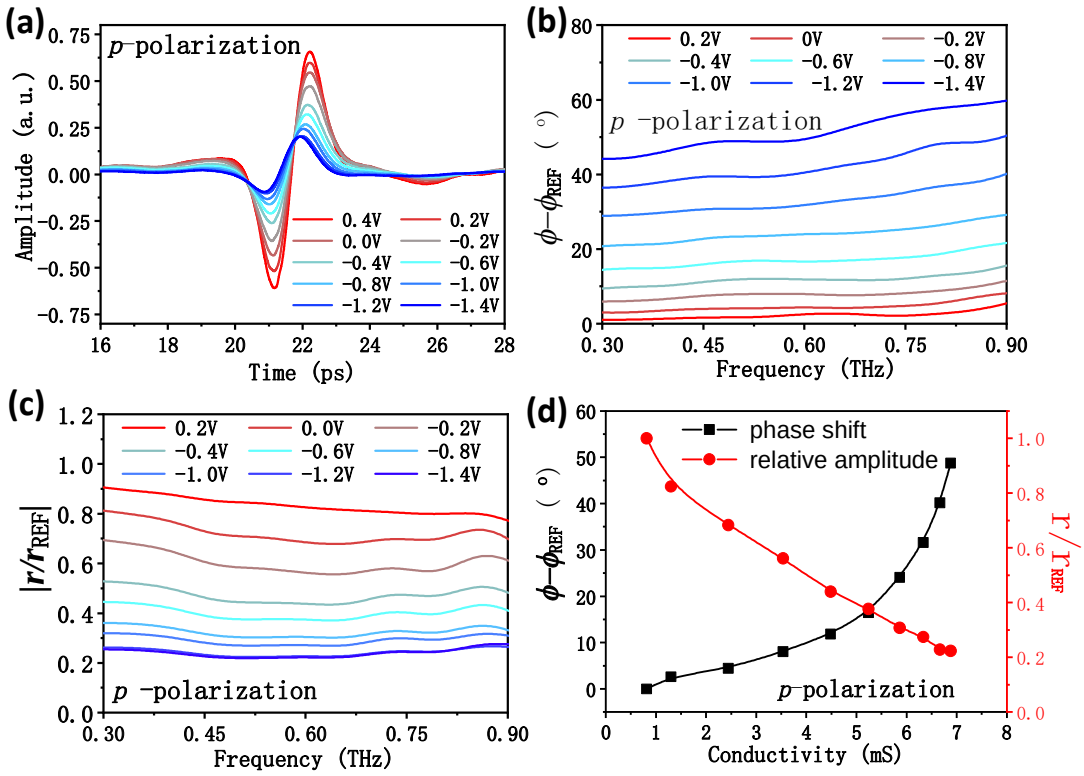

Figure 4 (a) Time domain THz waveforms of p-polarization under different gate voltages. (b) and (c) Phase modulations and reflection intensity (|r|) modulation. Data are obtained from (a) through Fourier transform and the result at the gate voltage of 0.4V is used as a reference. (d) phase shift and relative reflectance as function of conductivity.

We use polarization rotation angle ψ and the ellipticity angle χ to characterize the circular dichroism of the THz beam reflecting from our device. Polarization rotation angle ψ and the ellipticity angle χ can be extracted from the two orthogonal electromagnetic waves E_x and E_y:

$\tan(2\psi) = \frac{2A_xA_y cos\Delta\phi}{A_x^2 - A_y^2}$ and $\sin(2\chi) = \frac{2A_xA_y sin\Delta\phi}{A_x^2 + A_y^2}$. A_x and A_y are the amplitudes of the two orthogonal electromagnetic waves E_x and E_y, which correspond to the s- and p-polarization wave in our experiment. $\Delta\phi$ are the phase difference between E_x and E_y. The results are shown in figure 5(a) and (b). Different from polarization modulators based on metal resonance structure, which only exhibit high performance at certain frequencies, both the ψ and χ in our experiment show a broadband characteristic, from 0.3THz to 0.9THz. Specially, the ellipticity angle χ is spectrum-flat tunable and can be modulated from around -37° to 23°, which means the THz wave within this frequency can be tuned with the same chirality. Taking 0.6THz as an example, the polarization rotation angle ψ fluctuates between -20° to -45° and the ellipticity angle χ is modulated from -37° to 30°, as shown in figure 5(c). Correspondingly, the electric-field trajectory of the THz wave can be switched from right elliptical polarization to near linear polarization, then to left elliptical polarization, as shown in figure 5(d) to (f).

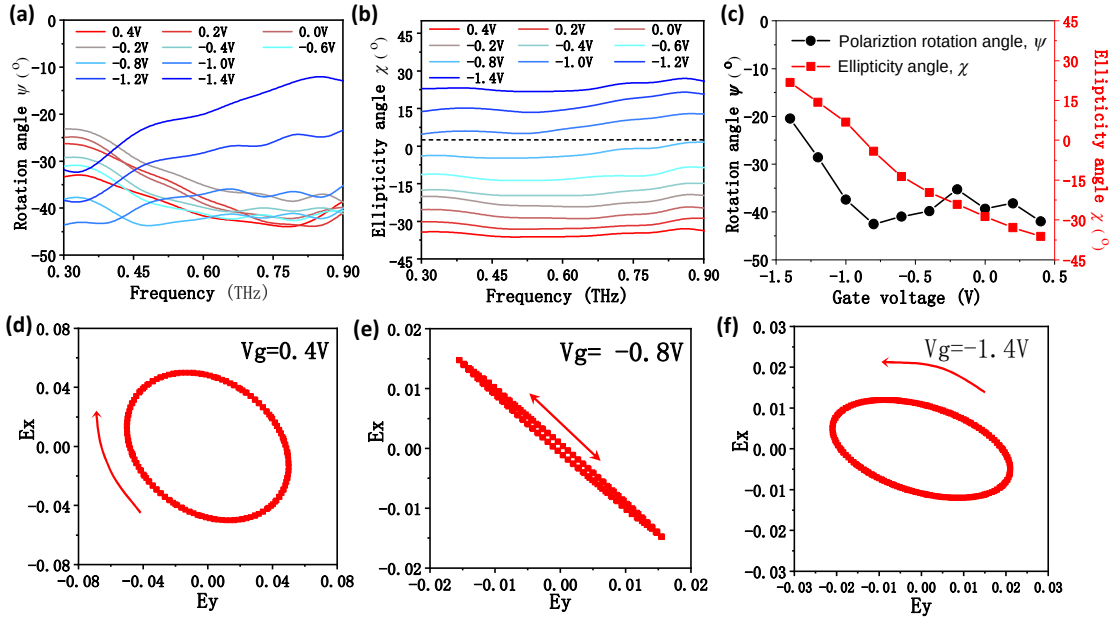

Figure 5 (a) the polarization rotation angle and (b) ellipticity angle under different gate voltages. (c) polarization rotation angle and ellipticity angle as function of gate voltage at the frequency of 0.6THz. (d), (e) and (f) are the projections of the electric-field trajectories at the frequency of 0.6THz for the gate voltage of 0.4V, -0.8V and -1.4V, respectively.

Terahertz pulse in time domain can be seen as the sum of THz wave with different frequencies. Therefore, to realize terahertz pulse shaping in time domain, a broadband electro-optic polarization conversion is required. Different from narrowband polarization converter based on metal resonance structures (such as metamaterials), our device has an ultra-broadband response, as shown in figure S3(a), (e) and (i) of the supporting information S3. This broadband response enables us to shape the polarization of THz waveforms in the time domain. Here, for the first time, by using the above THz polarization converter, we realized terahertz pulse shaping through electrical manipulation in the time domain. Figure 6(a), (b) and (c) show the experimentally obtained electric-field trajectories of the terahertz polarization-shaped waveforms under different gate voltages. The terahertz polarization-shaped waveform is composed of its two orthogonal

components $E_x(t)$ and $E_y(t)$, which correspond to s- and p- polarization, respectively. When a gate voltage of 0.4 V (corresponding to the conductivity of 0.9 mS) is applied, a heart-shaped elliptical pulse shape is observed, together with rotating clockwise with time to observer (which is corresponding to right hand circular polarization). This is because the phase difference between the s- and p- polarization is about -110° throughout the bandwidth, which results in an elliptically polarized THz wave for each frequency in this region. The polarization property for a single frequency (e.g. 0.3 THz, 0.6 THz, and 0.9 THz) is shown in the supporting information figure S3(a)-(d) . At V_g = -0.8 V, the THz pulse becomes linearly polarized, as a result of the phase difference of around 180° (supporting information figure S3(e) - (h)). If a gate voltage of -1.4 V is applied, the waveform becomes an elliptical heart-shape and rotates anticlockwise with time to observer (which is corresponding to left hand circular polarization), because the phase difference is around 230° (supporting information figure S3(i)- (l)). It is worth mentioning that the terahertz polarization-shaped pulses above were realized by a simple set-up and more waveforms can be achieved through changing the incident angle and graphene's structure (such as a graphene grating).

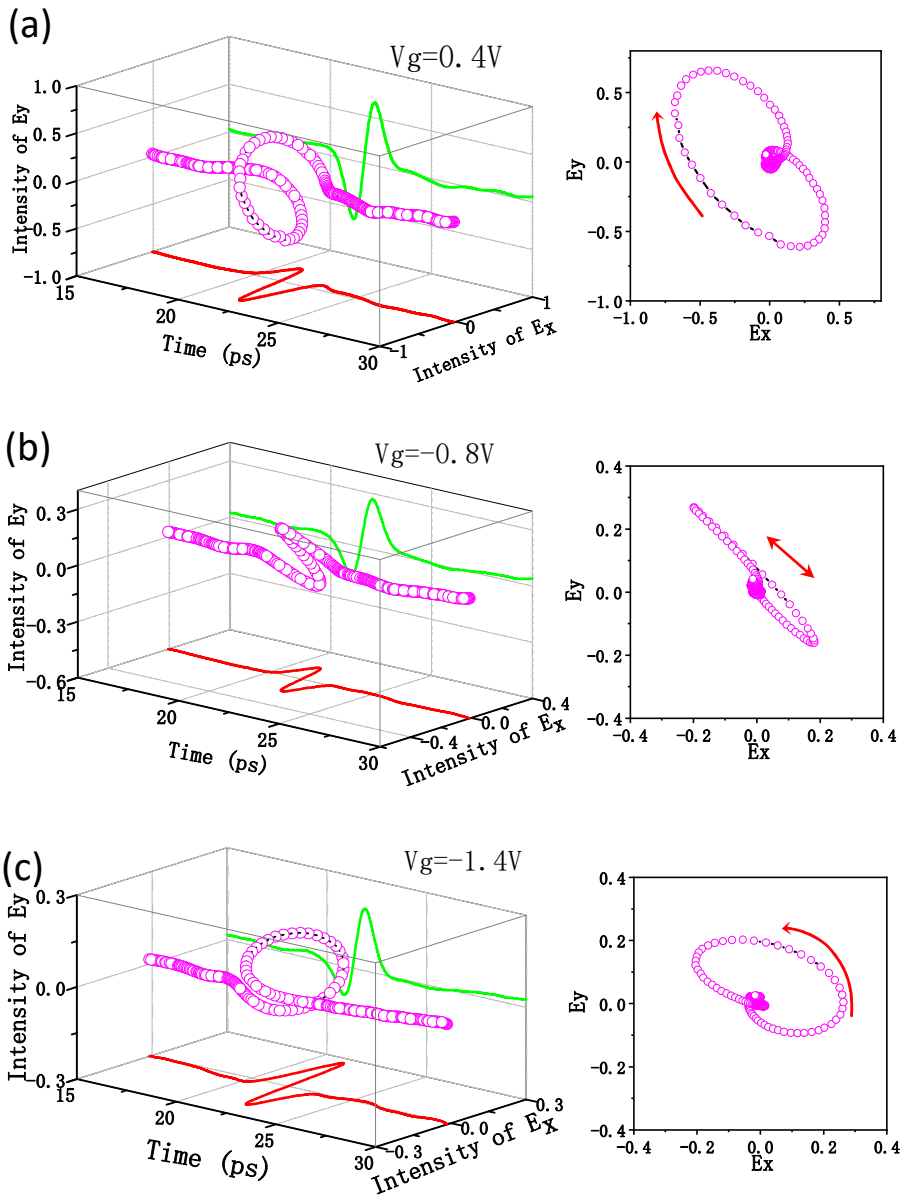

Figure 6 Electric-field trajectories of the terahertz polarization-shaped waveform (left) and the projections on the Ex-Ey plane (right) under gate voltages of (a) 0.4 V, (b) -0.8V and (c) -1.4V.

Conclusion

In summary, we present a highly tunable and ultra-broadband THz polarization converter constructed with atomic-layer graphene and a TIR prism which exploits the phase change effect to achieve efficient modulation. Theoretical analysis and experimental results verify that the reflection system can be switched from TIR to MMR by controlling the conductivity of graphene and show an ultra-broadband THz polarization modulation. In addition, the electrical control of THz pulse shape in time domain is also demonstrated. Compared with the previous graphene THz devices [34-40], our device shows an ultra-broad band response and a small dispersion, because both the total internal reflection and the mirror reflection are not resonant-based. Experimental results show a working bandwidth of 0.3-0.9THz (the ratio between the bandwidth and frequency center is about 1.5). Another advantage is the low working voltage offered by the high capacitance of the ion-gel gate. The proposed device can be used in adaptive optimization of broadband THz waveforms, showing a great potential for numerous applications in both physics and biology.

Method

Device fabrication

Two monolayer Graphene sheets are transferred to a quartz (1.5cm*1.5cm) one by one by standard wet transfer method. After that, photolithography was used as a mask to define the position of electrodes and Cr/Au (5nm/80nm) films were deposited as electrodes by thermal evaporation deposition technique. More detail about the device fabrication is shown in supporting information S4.

The ion-gel was fabricated by mixing 1-ethyl-3-methylimidazolium bis(trifluoromethylsulfonyl)imide ([EMIM][TFSI]) ionic liquid, PVDF-EVA and acetone with a ratio of 1 : 4 : 7 (w/w). This solution was drop-cast on silicon wafer and annealing with temperature of 350K. Then the ion-gel film was lift off from wafer and transferred to the prepared graphene/quartz. When doing measurement, then this ion-gel/graphene/quartz device was put on a quartz prism. More details are shown in the supporting information S4 and the stability of ion-gel also be discussed in the supporting information S5.

Terahertz measurements

A THz-TDS system from Menlo Systems (TERA-K15) is used for the terahertz reflection measurements. A reflection guide is used for manual adjustment of the reflection angle of 45°.

Funding Sources The work is in part supported by Research Grants Council of Hong Kong, particularly, via Grant Nos. AoE/P-701/20, 14203018, N_CUHK438/18, and CUHK Group Research Scheme, and CUHK Postdoctoral Fellowship by Innovation and Technology Commission, Hong Kong SAR Government and partially supported by the National Natural Science Foundation of China (62104165, 61988102), the Natural Science Foundation of Jiangsu Province (BK20210713), Gusu Youth Leading Talent ZXL2021452. K.C thanks the support by National Natural Science Foundation of Guangdong for Distinguished Young Scholars (Grant No. 2018B030306043); Pearl River Talent Plan (Grant No. 2019QN01C109); The Fundamental Research Funds for the Central Universities, Sun Yat-sen University (Grant No. 22qntd0503); State Key Laboratory of Optoelectronic Materials and Technology Independent subject (Grant No. OEMT-2022-ZRC-06). M.L thanks the support by

the Natural Science Foundation of Guangdong Province (No.2019B151502028)

References

[1] Wai Lam Chan, Jason Deibel & Daniel M. Mittleman, Imaging with terahertz radiation, Report of Progress in Physics 70, 1325 (2007)

[2] Masayoshi Tonouchi, Cutting-edge terahertz technology, Nature Photonics, 1, 97 (2007)

[3] Tadao Nagatsuma, Guillaume Ducournau & Cyril C. Renaud, Advances in terahertz communications accelerated by photonics, Nature Photonics 10, 371–379 (2016)

[4] S. Koenig, et al., Wireless sub-THz communication system with high data rate, Nature Photon 7, 977 (2013)

[5] Marco Rahm & Jiu-Sheng Li & Willie J. Padilla, THz Wave Modulators: A Brief Review on Different Modulation Techniques, Journal of Infrared and Millimetre Terahertz Waves 34, 1–27 (2013)

[6] Mitttleman, D. M., Cunningham, J., Nuss, M. C. & Geva, M. Noncontact semiconductor wafer characterization with the Hall effect. Appl. Phys. Lett. 71, 16–18 (1997)

[7] Markelz, A.G., Roitberg, A. & Heilweil, E.J. Pulsed terahertz spectroscopy of DNA, bovine serum albumin and collagen between 0.1 and 2.0 THz. Chem. Phys. Lett. 320, 42–48 (2000)

[8] Shao, J. & Hänggi, P. Control of molecular chirality. J. Chem. Phys. 107, 9935 (1997).

[9] Won Jin Choi, et al., Chiral phonons in microcrystals and nanofibrils of biomolecules, Nature Photonics, 16, 366–373 (2022)

[10] van der Valk, N. C. J., van der Marel, W. A. M. & Planken, P. C. M. Terahertz polarization imaging. Opt. Lett. 30, 2802–2804 (2005)

[11] Ranjan Singh, Eric Plum, Weili Zhang, and Nikolay I. Zheludev, Highly tunable optical activity in planar achiral terahertz metamaterials, Opt. Express 18, 13425-13430 (2010)

[12] E. Feigenbaum, K. Diest, H. A. Atwater, Unity-order index change in transparent conducting oxides at visible frequencies. Nano Lett. 10, 2111–2116 (2010)

[13] Kersting, R., Strasser, G. & Unterrainer, K. Terahertz phase modulator. Electron. Lett. 36, 1156–1158 (2000).

[14] Yong Zhi Cheng, Withawat Withayachumnankui, et al., Ultrabroadband reflective polarization convertor for terahertz waves, Appl. Phys. Lett. 105, 181111 (2014)

[15] A. H. Dorrah, N. A. Rubin, A. Zaidi, M. Tamagnone, F. Capasso, Metasurface optics for on-demand polarization transformations along the optical path. Nat. Photonics 15, 287–296 (2021)

[16] NATHANIEL K. GRADYJANE E. HEYES, et al., Terahertz Metamaterials for Linear Polarization Conversion and Anomalous Refraction, SCIENCE, 6138. 1304-1307 (2013)

[17] Choi, W.J., Cheng, G., Huang, Z. et al. Terahertz circular dichroism spectroscopy of biomaterials enabled by kirigami polarization modulators. Nat. Mater. 18, 820–826 (2019).

[18] Shuang Zhang, Jiangfeng Zhou, et al. Photoinduced handedness switching in terahertz chiral metamolecules, Nature Communications 3, 942 (2012)

[19] He, J., Dong, T., Chi, B. et al. Metasurfaces for Terahertz Wavefront Modulation: a Review. J Infrared Milli Terahz Waves 41, 607–631 (2020).

[20] Kan, T. et al. Enantiomeric switching of chiral metamaterial for terahertz polarization modulation employing vertically deformable MEMS spirals. Nat. Commun. 6, 8422 (2015).

[21] A. H. Castro Neto, F. Guinea, N. M. R. Peres, K. S. Novoselov, & A. K. Geim. The electronic properties of graphene, Reviews of Modern Physics 81, 109 (2009).

[22] S. Das Sarma, S. Adam, E. H. Hwang, & E. Rossi, Electronic transport in two dimensional graphene, Reviews of Modern Physics 83, 407 (2011)
[23] Berardi Sensale-Rodriguez, et al., Broadband graphene terahertz modulators enabled by intraband transitions, Nature Communications 3, 780 (2012)
[24] Chen, Z., Chen, X., Tao, L. et al. Graphene controlled Brewster angle device for ultra broadband terahertz modulation. Nat Commun 9, 4909 (2018).
[25] Yury Malevich, M. Said Ergoktas, Gokhan Bakan, Pietro Steiner, and Coskun Kocabas, Video-Speed Graphene Modulator Arrays for Terahertz Imaging Applications, ACS Photonics 2020, 7, 9, 2374–2380
[26] Seung Hoon Lee, et al, Switching terahertz waves with gate-controlled active graphene metamaterials, Nature Materials 11, 936 (2012)
[27] Ziqi Miao, Qiong Wu, Xin Li, Qiong He, Kun Ding, Zhenghua An, Yuanbo Zhang, and Lei Zhou, Widely Tunable Terahertz Phase Modulation with Gate-Controlled Graphene Metasurfaces, Phys. Rev. X 5, 041027(2015)
[28] Nikolaos Matthaiakakis,et al., Dynamic Control of Light Chirality with Nanostructured Monolayer Black Phosphorus for Broadband Terahertz Applications, Advanced Optical Materials, 5, 2102273(2022)
[29] SOUVIK BISWAS, et al., Broadband electro-optic polarization conversion with atomically thin black phosphorus, Science, 6566, 448-453(2021)
[30] Yuanyuan Huang, et al., Tunable circular polarization conversion and asymmetric transmission of planar chiral graphene-metamaterial in terahertz region, Carbon, 119, 305-313, 2017
[31] Nikolaos Matthaiakakis, Boundary Element Method Simulations of Tunable Chiral Radiation and Active Chirality Switching from Rectangular Graphene Nanosheets: Implications for Dynamic Control of Light Chirality, ACS Appl. Nano Mater. 3, 7, 6816–6826 (2020)
[32] Stephen J. Kindness, Nikita W. Almond, et al. A Terahertz Chiral Metamaterial Modulator, Adv. Optical Mater.2020, 8, 2000581
[33] Masyukov, M., Vozianova, A., Grebenchukov, A. et al. Optically tunable terahertz chiral metasurface based on multi-layered graphene. Sci Rep 10, 3157 (2020).
[34] Kim et al. Electrical access to critical coupling of circularly polarized waves in graphene chiral metamaterials, Sci. Adv. 2017;3: e1701377
[35] Teun-Teun Kim, Hyunjun Kim, et al. Amplitude Modulation of Anomalously Refracted Terahertz Waves with Gated-Graphene Metasurfaces, Adv. Optical Mater.2018, 6, 1700507
[36] M. Amin, O. Siddiqui, and M. Farhat, Linear and Circular Dichroism in Graphene-Based Reflectors for Polarization Control, Phys. Rev. Applied 13, 024046 (2020)
[37] Rui Zhang, Bing You, et al., Broadband and switchable terahertz polarization converter based on graphene metasurfaces, Opt. Express 29, 24804-24815 (2021)
[38] Tun Cao, Yang Li, et al., Theoretical study of tunable chirality from graphene integrated achiral metasurfaces, Photon. Res. 5, 441-449 (2017)
[39] Alessandra Di Gaspare, Tunable, Grating-Gated, Graphene-On-Polyimide Terahertz Modulators, Adv. Funct. Mater. 31, 2008039 (2021)
[40] Yongzhi Cheng, Jinxiu Wang, Tunable terahertz circular polarization convertor based on graphene metamaterial, Diamond and Related Materials, 119, 108559, 2021
[41] Yongzhi Cheng, Xuzheng Zhu, Jun Li, Fu Chen Hui Luo, Ling Wu, Terahertz broadband tunable reflective cross-polarization convertor based on complementary cross-shaped graphene

metasurface, Physica E: Low-dimensional Systems and Nanostructures, 134, 114893, 2021

[42] Jiaqi Liu, Yongzhi Cheng, Fu Chen, Hui Luo, and Xiangcheng Li, High-efficiency reflective metasurfaces for terahertz vortex wave generation based on completely independent geometric phase modulations at three frequencies, Journal of the Optical Society of America B, 39(7), 1752-1761, 2022

[43] Broadband tunable terahertz metasurface absorber based on complementary-wheel-shaped graphene, Yongzhi Cheng, Haolin Zhao, Chan Li, Optical Materials, 109, 110369, 2020

[44] Xuzheng Zhu, Yongzhi Cheng, Junpeng Fan, Fu Chen, Hui Luo, Ling Wu, Switchable efficiency terahertz anomalous refraction and focusing based on graphene metasurface, Diamond and Related Materials, 121, 108743, 2022

[45] Xuzheng Zhu, Yongzhi Cheng, Fu Chen, Hui Luo, and Wu Ling, Efficiency adjustable terahertz circular polarization anomalous refraction and planar focusing based on a bi-layered complementary Z-shaped graphene metasurface, Journal of the Optical Society of America B 39(3), 705-712 (2022)

[46] Fu Chen, Yongzhi Cheng, and Hui Luo, A Broadband Tunable Terahertz Metamaterial Absorber Based on Single-Layer Complementary Gammadion-Shaped Graphene, Materials, 13, 860, 2020

[47] Soo Min Kim, et al, Synthesis of large-area multilayer hexagonal boron nitride for high material performance, Nature Communications, 6, 8662 (2015)

[48] Junku Liu, et al., Enhanced performance of graphene transistor with ion-gel top gate, Carbon 68, 480-486, 2014

[49] Beom Joon Kim, et al., High-Performance Flexible Graphene Field Effect Transistors with Ion Gel Gate Dielectrics, Nano Lett., 10, 9, 3464–346, 2010

ToC

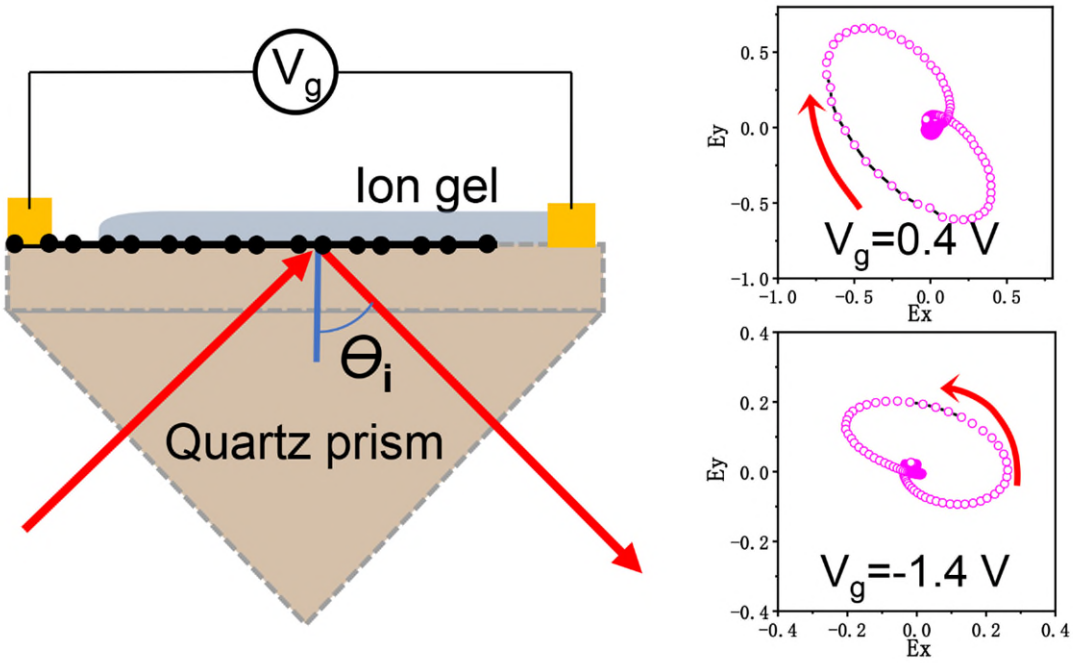

A graphene-ion gel gated structure on a quartz prism enables broadband electric-optic chiral polarization conversion for reshaping Terahertz pulse in time-domain.